RSC Advances

PAPER

View Article Online
View Journal | View Issue

Cite this: *RSC Adv.*, 2019, **9**, 5354

Novel red-emitting phosphor $Li_2MgZrO_4:Mn^{4+},Ga^{3+}$ for warm white LEDs based on blue-emitting chip

Wen Yan, Siguo Xiao * and Xiaoliang Yang

Received 3rd December 2018
Accepted 27th January 2019

DOI: 10.1039/c8ra09933b

rsc.li/rsc-advances

$Li_2MgZrO_4:Mn^{4+},Ga^{3+}$ phosphors are synthesized *via* a conventional high-temperature solid-state reaction. The red emission of Mn^{4+} is enhanced 6.68 times and 13.0 times under 352 nm and 468 nm excitation when Ga^{3+} ions with a concentration of 40% are introduced into the phosphor. The thermal stability of the phosphor is also slightly improved by Ga^{3+} doping. It is believed that the Ga_{Zr} dopants in the Li_2MgZrO_4 host not only stabilize Mn ions in the 4+ state, but also lower the symmetry of Mn^{4+} sites, resulting in the significant improvement of the luminescence performance, especially under blue excitation. The results might provide meaningful reference to seek high-performance Mn^{4+} doped oxide phosphors for W-LED applications based on a blue-emitting InGaN chip.

1. Introduction

White light emitting diodes (W-LEDs) have sparked great interests due to their superior properties in luminous efficiency, lifetime, reliability, and environment-friendly features.[1–4] Presently most W-LEDs are fabricated by an InGaN LED (emitting near 460 nm) in combination with a yellow emitting phosphor such as $Y_3Al_5O_{12}:Ce^{3+}$ (YAG:Ce^{3+}).[5,6] However, their luminescence suffers from problems such as cold white light and a low color-rendering index, which results from the lack of red spectral contribution.[7–9] In order to obtain white light with a high-color-rendering index (CRI, Ra $\geq$ 80) and low correlated color temperature (CCT $\leq$ 4500 K), suitable red phosphors need to be mixed with YAG:Ce^{3+}.[10,11] Great efforts have been made to exploit novel rare-earth-doped red phosphors with high efficiency for this purpose, and the most successful materials are Eu^{2+}- or Ce^{3+}-doped nitride compounds.[12–14] Regretfully, because of the 4f–5d transitions, the light re-absorption in the green or yellow spectral region for these nitride phosphors is unavoidable, causing color change and luminous reduction of W-LEDs.[15] Besides, the red-emitting nitride phosphors are quite expensive due to the complex synthesis procedures.[15,16]

As an alternative, the non-rare-earth Mn^{4+} doped red phosphors have gained increased attention recently due to their low cost and admirable spectral features. They usually exhibit broad and strong absorption between 250 and 550 nm and emit efficiently light from 600 to 750 nm.[17–22] So far, Mn^{4+} red luminescence has been reported in Mn^{4+}-doped fluoride and oxide compounds. For Mn^{4+} activated fluorides, they exhibit intense excitation band centered at ~460 nm and sharp red emission lines peaking at ~630 nm.[6,23–25] Regretfully, the fluoride host is not stable due to its hygroscopicity. Moreover, in the synthesis process the required toxic HF solution is very harmful to environment.[22,23] In contrast, Mn^{4+} activated oxides exhibiting much high chemical stability with an eco-friendly preparation procedure, show promising capabilities as good red converters for warm W-LEDs.[26–28] Mn^{4+} activated aluminates,[29,30] titanates,[31,32] germanates[33] and pyrosilicates[34–38] has been widely reported. Unfortunately, the currently known Mn^{4+} activated oxide phosphors cannot meet the needs of general lighting due to the low quantum efficiency (QE) when excited by blue chips. Hence more in-depth investigations on Mn^{4+} activated oxide phosphors to improve their red luminescence performance are highly desired. Just recently the luminescence properties of Mn^{4+} activated double perovskites oxide Li_2MgZrO_4 (LMZO) have been reported.[39] LMZO contains [ZrO_6] octahedrons, offering great capacity to accept Mn^{4+} substitutes, thereupon efficient red emission is observed under excitation of both UV and blue light. The aim in the current study, therefore, is to enhance the red emission intensity of Mn^{4+} in LMZO host, especially under blue light excitation, by doping with an impurity of Ga^{3+}.

2. Experimental section

2.1. Sample fabrication

The LMZO:Mn^{4+},Ga^{3+} powders were prepared by a conventional high-temperature solid-state reaction method. The chemicals, such as Li_2CO_3 (A.R. 99.5%), MgO (A.R. 99.9%), ZrO_2 (A.R. 99.9%), $MnCO_3$ (A.R. 99.5%), and Ga_2O_3 (99.5%) are used as raw materials, which are purchased from the Aladdin Chemical Reagent Company in Shanghai, China. The nominal chemical compositions for the phosphors were designed as $Li_2MgZr_{0.996-x}O_4:Mn_{0.004}^{4+},Ga_x^{3+}$ (x = 0.00, 0.05, 0.10, 0.15, 0.20, 0.25, 0.30, 0.35, 0.40, 0.45, 0.50). The starting materials were

School of Physics and Optoelectronics, Xiangtan University, Hunan 411105, China. E-mail: Xiaosiguo@xtu.edu.cn; Fax: +8673158292468; Tel: +8613786239082

weighed with stoichiometric ratio and finely mixed in an agate mortar to ensure homogeneous mixing. Then the mixed samples were sintered at 1250 °C for 8 h in air. After that, the samples were cooled to room temperature and finely ground to obtain the final products.

2.2. Characterization

The crystalline phases of the samples were analyzed by X-ray diffraction (XRD) on a Bruker D8 advanced equipment, using Cu tube with Cu/K ($k = 0.1541$ nm) radiation in the 2θ range of 5° to 90°. The photoluminescence excitation spectra and visible-NIR photoluminescence spectra were measured by a monochromator (Zolix Instrument, Omni-λ320i) coupled with photomultiplier tube (PMTHS1-R928), in which a monochromator (Zolix Instrument Omni-λ300) coupled with a 150 W xenon lamp was used to provide monochromatic light for excitation spectra measurement. Luminescence decay curves and temperature dependent emission spectra were measured by a FLS920 (Edinburgh) spectrometer. Both continuous and pulsed 150 W xenon lamps were used as excitation light source and an R928p (hamamatsu) detector was used to acquire emission light signal. Quantum efficiency (QE) is measured directly by a Mars HS3000 spectrofluorimeter with integrating sphere at room temperature.

3. Results and discussion

3.1. Crystal structure analysis

The X-ray diffraction (XRD) patterns of the as-prepared LMZO:$Mn_{0.004}^{4+}$,Ga_x^{3+} (x = 0.00, 0.05, 0.10, 0.15, 0.20, 0.25, 0.30, 0.35, 0.40, 0.45, 0.50) are shown in Fig. 1. The XRD pattern of the sample doped with relatively low Ga^{3+} concentration ($x \leq 0.40$) matches well with the Joint Committee on Powder Diffraction Standard (JCPDS) card 78-0198 for LMZO. This indicates that the introduction of Ga^{3+} ions within a certain concentration range has not caused significant change in the crystal structure of the LMZO. However, impurity phases such as MgO, and $LiGaO_2$ appears as the doped Ga^{3+} ions is high enough ($x > 0.40$). A schematic of the LMZO crystal structure is also given in Fig. 2. LMZO as a double perovskites oxide is described as the tetragonal crystal system with space-group $I4_1/amd$ (141).[40] The LMZO crystal structure consists of [LiO_4] tetrahedron, [MgO_6] and [ZrO_6] octahedral. Mn^{4+} ions tend to replace the Zr^{4+} sites in terms of the charge balance and ionic radius similar principle.[41] Meanwhile, the XRD analysis suggests that the sample remains pure LMZO when the doped Ga^{3+} concentration is less 40%, meaning that substitution of Zr^{4+} by Ga^{3+} in LMZO is also permissible. When Ga^{3+} ions replace the Zr^{4+} ions, oxygen vacancies might form to keep the electroneutrality of the compound.

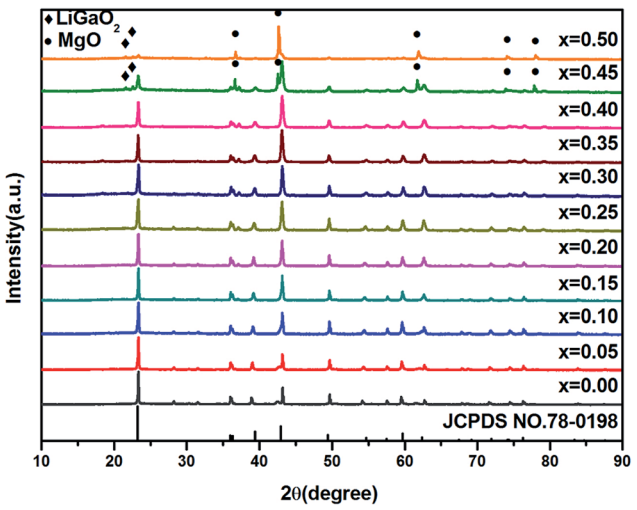

Fig. 1 XRD patterns of LMZO:$Mn_{0.004}^{4+}$,Ga_x^{3+} (x = 0.00, 0.05, 0.10, 0.15, 0.20, 0.25, 0.30, 0.35, 0.40, 0.45, 0.50) phosphors.

More detailed morphological and compositional results of the as-synthesized LMZO:$Mn_{0.004}^{4+}$,$Ga_{0.40}^{3+}$ powder obtained from SEM and EDS measurements are shown in Fig. 3. Fig. 3a displays the fine particles with irregular and polygonal-shape morphology and the sizes in the range of sub-micrometer to a few micrometers. In the corresponding EDS spectrum presented in Fig. 3b, the peaks of manganese (Mn), magnesium (Mg), gallium (Ga), zirconium (Zr) and oxygen (O) can be clearly identified. As shown in Table 1, the atomic ratio of the three elements of Zr, Mn and Ga is calculated to be substantially equal to the stoichiometric ratio, which further suggests that Mn and Ga elements have indeed successfully occupied the lattice sites of Zr, generated the substance we expected.

3.2. Characteristic analysis

Fig. 4 shows the photoluminescence excitation (PLE) spectra of LMZO:$Mn_{0.004}^{4+}$,Ga_x^{3+} (x = 0.00, 0.40) samples, which were recorded by monitoring the red emission at 670 nm. In the region from 300 to 550 nm, the PLE spectra for both Ga^{3+} doped and un-doped samples consist of two broad excitation bands peaking at 352 and 468 nm, respectively. The PLE band in the near ultraviolet-violet range includes two overlapping excitation bands which originate from the Mn^{4+}–O^{2-} charge transfer (CT) and $^4A_2 \rightarrow {}^4T_1$ transition of Mn^{4+} ion, respectively, while the band in the blue-green range is attributed to the $^4A_2 \rightarrow {}^4T_2$ transition of Mn^{4+} ions.[42,43] It is found that the introduction of

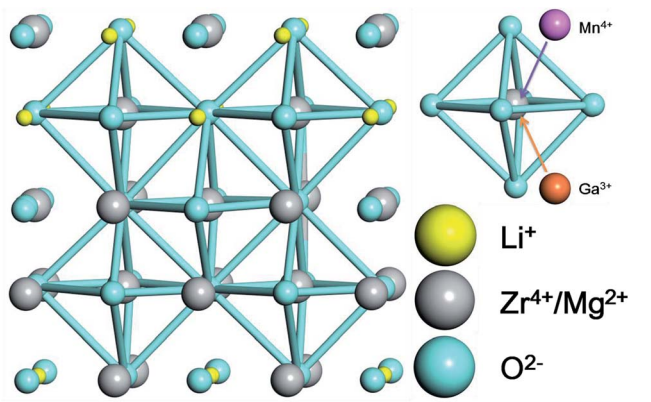

Fig. 2 Schematic of the LMZO crystal structure.

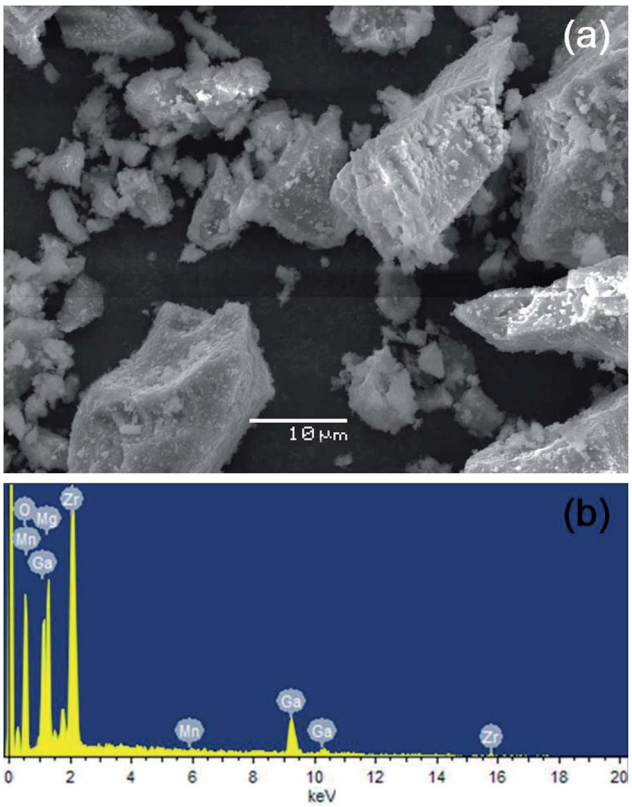

Fig. 3 (a) SEM image and (b) EDS results of the LMZO:$Mn_{0.004}^{4+}$,-$Ga_{0.40}^{3+}$ powder.

Table 1 EDS results of the LMZO:$Mn_{0.004}^{4+}$,$Ga_{0.40}^{3+}$ powder

Chemical element	Weight percentage	Atomic percentage
O	37.06	67.75
Mg	11.64	14.01
Mn	0.04	0.02
Ga	18.03	7.56
Zr	33.23	10.66

Ga^{3+} ions has significantly changed excitation properties of Mn^{4+} ions, just as shown in the inset (a) of Fig. 4. From Fig. 4, one may find that the excitation intensities at 352 and 468 nm both increase with Ga^{3+} doping concentration increasing, reaches their maximum at $x = 0.40$, and then decrease sharply when the Ga^{3+} concentration is higher than 40 mol%. At $x = 0.40$, the excitation intensity at 352 nm is enhanced by 6.85 times, while the excitation intensity at 468 nm is enhanced by 10.6 times. This suggests that the excitation intensity in both ultraviolet-violet and blue-green range can be largely enhanced by introduction of Ga^{3+} ions of suitable concentration. However, the doped Ga^{3+} ions can more effectively improve the excitation properties in the blue-green region as compared with that in the ultraviolet-violet region, which can been clearly seen from the inset (b) in Fig. 4. The inset (b) in Fig. 4 gives the ratio of excitation intensity at 468 nm to that at 352 nm as a function of Ga^{3+} concentration. It is found that the ratio increases from 1.17 to 2.00 as Ga^{3+} doping concentration increases from 0% to 50%.

The measured photoluminescence (PL) spectra of LMZO:$Mn_{0.004}^{4+}$,Ga_x^{3+} ($x = 0.00$, 0.40) phosphors under excitation of 352 and 468 nm are shown in Fig. 5. The emission spectra for Ga^{3+} doped and un-doped samples show similar profiles whether excited by 365 nm or 468 nm light, except for the intensity. They present a broad band in the region of 610–800 nm with emission peak at about 670 nm, corresponding to the $^2E \rightarrow {}^4A_2$ transition of Mn^{4+} ions.[44,45] The full-width at half maximum (FWHM) of the Mn^{4+} emission band for these powders is about 40 nm. The Ga^{3+} concentration dependent emission intensity upon 352 nm and 468 nm excitation is shown in the inset of Fig. 5. The highest photoluminescence intensity is achieved at Ga^{3+} doping concentration of 40 mol% ($x = 0.40$) and it is enhanced by 6.68 times and 13.0 times under 352 nm and 468 nm excitation as compared with the Ga^{3+} un-doped sample, respectively.

Based on the PL spectra, the Commission Internationale de L'Eclairage (CIE) coordinate for the phosphors can be calculated. The CIE coordinate has little altered when the sample is doped with Ga^{3+} ions of different concentration, since the doped Ga^{3+} ions has not changed the spectral shape of the emission band. The CIE coordinates for all the samples excited at 468 nm are (0.726, 0.274), located in the deep-red region. Fig. 6 shows the CIE coordinate of the phosphors under 468 nm excitation. The digital images of the as-prepared LMZO:$Mn_{0.004}^{4+}$,Ga_x^{3+} ($x = 0.00$, 0.05, 0.10, 0.15, 0.20, 0.25, 0.30, 0.35, 0.40, 0.45, 0.50) phosphors under daylight and 365 nm near-UV light are also given in Fig. 6. The daylight color of the samples changes from shallow to deep with an increase of the Ga^{3+} concentration. The red emissions from LMZO:$Mn_{0.004}^{4+}$,Ga_x^{3+} upon 365 nm excitation can be clearly seen with the naked eye. The color under 365 nm near ultraviolet light of the samples changes from dark to light and then from light to dark with the increase of the Ga^{3+} concentration. The light reaches the brightest when $x = 0.40$.

In recent years, many new Mn^{4+} doped oxide phosphors have been developed and some Mn^{4+} doped oxide phosphors reported can give very efficient red or deep red emission under near ultraviolet excitation.[46–49] Regretfully, their emission intensities under blue excitation are usually much weaker than that under near ultraviolet excitation. This makes it difficult to meet the need of W-LEDs application based on blue-emitting InGaN chip. In the present work, however, it is manifested that the emission intensity of Mn^{4+} in the LMZO host can be significantly improved by Ga^{3+} doping, especially excited the blue light. This provides import reference for finding new Mn^{4+} doped oxide phosphors matching with the commercial blue chips.

It is known that the electronic states of $3d^3$ configuration of Mn^{4+} are even, and because of this, the transitions between these states are forbidden in the electric-dipole approximation. This rule can be somewhat released by an admixture of the states of opposite parities. In the LMZO host, the Ga^{3+} doping might lower the symmetry of Mn^{4+} sites and thus the admixture of states of opposite parity would increase. As a result, the electric dipole amplitude of Mn^{4+} arises with the increase of Ga^{3+} doping content. This might lead to large increase of the

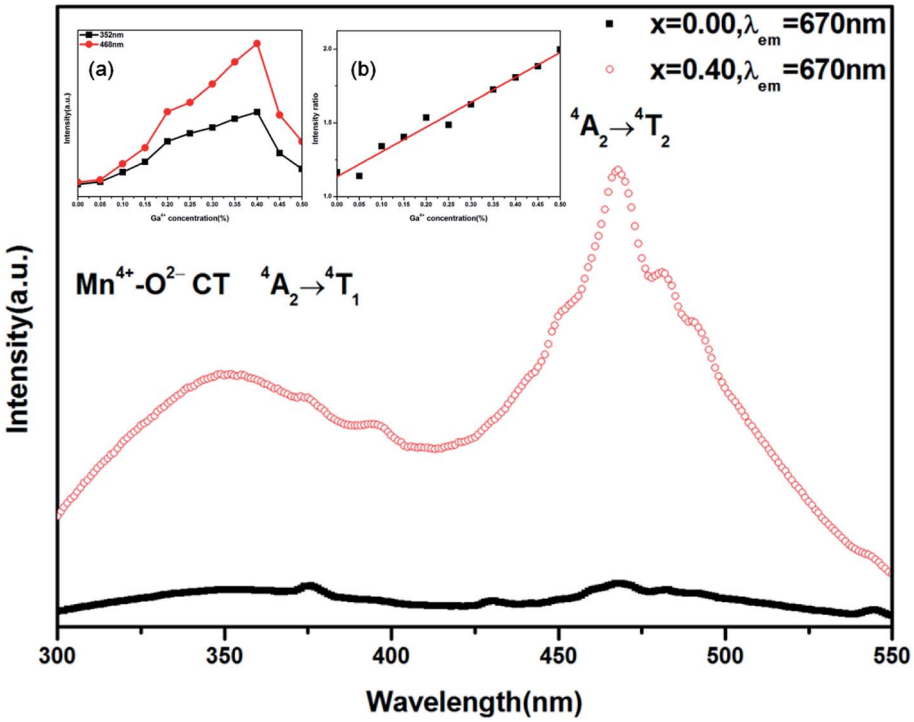

Fig. 4 PLE spectra of LMZO:$Mn_{0.004}^{4+}$,Ga_x^{3+} (x = 0.00, 0.40) phosphors at room temperature (λ_{em} = 670 nm). The inset (a) the relationship between the excitation intensity at 352 nm and 468 nm with the doping concentration of Ga^{3+}. The inset (b) the ratio of excitation intensity at 468 nm to that at 352 nm as a function of Ga^{3+} concentration.

Mn^{4+} red emission excited by blue light. However, the emission increase caused by Ga^{3+} doping under ultraviolet excitation is not as significant as that under blue excitation, since some contribution of ultraviolet excitation is provided by Mn^{4+}–O^{2-} charge transfer that should be less sensitive to the local environment. On the other hand, Ga_{Zr} dopants might also be

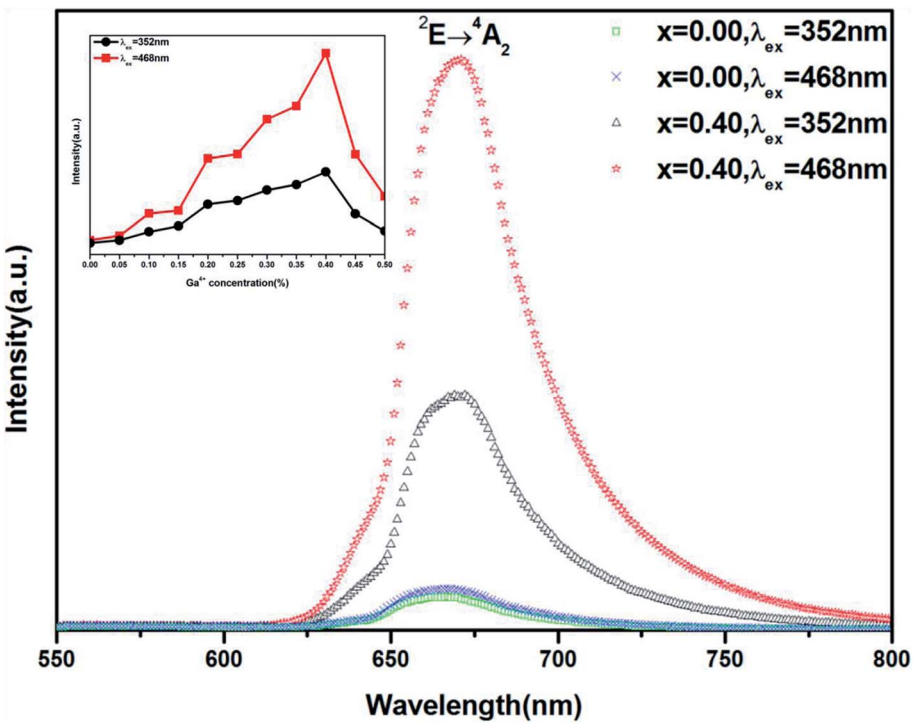

Fig. 5 Photoluminescence (PL) spectra of LMZO:$Mn_{0.004}^{4+}$,Ga_x^{3+} (x = 0.00, 0.40) phosphors under excitation of 352 and 468 nm. The inset: the relationship between emission intensity (λ_{ex} = 352 and 468 nm) and Ga^{3+} doping concentration.

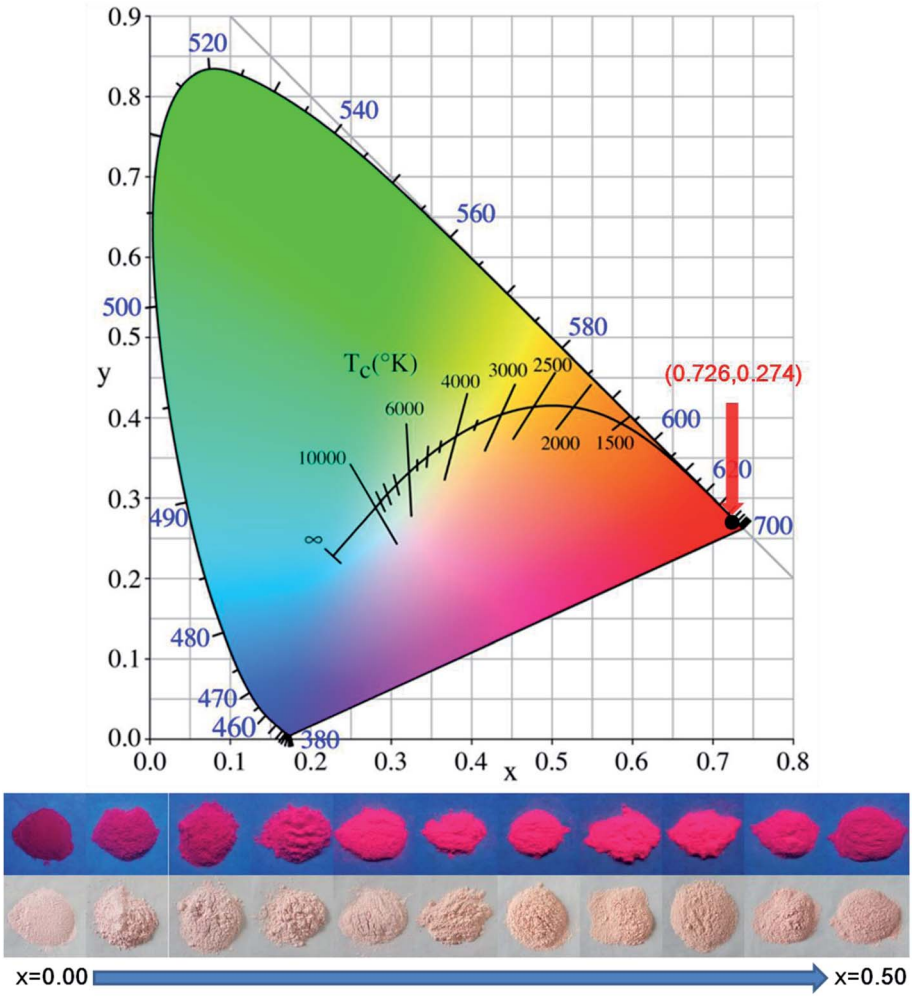

Fig. 6 CIE coordinate of the phosphors under 468 nm excitation and photographs of the LMZO:$Mn_{0.004}^{4+}$,Ga_x^{3+} ($x = 0.00$, 0.05, 0.10, 0.15, 0.20, 0.25, 0.30, 0.35, 0.40, 0.45, 0.50) phosphors with changing the concentration of Ga^{3+} under 365 nm UV (upper line) and visible light (lower line).

helpful to stabilize Mn ions in 4+ state and thus enhance the luminescence intensity of the phosphor. Near recent investigation shows that hole-type dopants in $Y_3Al_5O_{12}$ (YAG), such as Mg_{Al_6}, Ca_Y and Na_Y, can enhance the stability of Mn^{4+} state and correspondingly enhance its luminescence intensity.[50] Presumably Ga_{Zr} dopants might play the similar role in the LMZO host, stabilizing Mn^{4+} ions and reducing the formation of low valent Mn ions such as Mn^{3+}. This not only increases the required Mn^{4+} luminescence centres, but also reduces the luminescence quenching based on energy transfers such as $Mn^{4+} \rightarrow Mn^{3+}$. The reduced luminescence quenching might also be proven by the Ga^{3+} concentration dependent luminescence decay properties of the red emission.

The luminescence decay curves of the 670 nm red emission of $Li_2MgZr_{0.996-x}O_4$:$Mn_{0.004}^{4+}$,Ga_x^{3+} ($x = 0.00$, 0.05, 0.10, 0.15, 0.20, 0.25, 0.30, 0.35, 0.40, 0.45, 0.50) were measured under excitation of 468 nm light with pulsed duration of 1.5 μs, shown in Fig. 7. The mean lifetime τ_m can be calculated based on the formula:[51]

$$\tau_m = \frac{\int_0^\infty t \times I_{(t)} dt}{\int_0^\infty I_{(t)} dt} \quad (1)$$

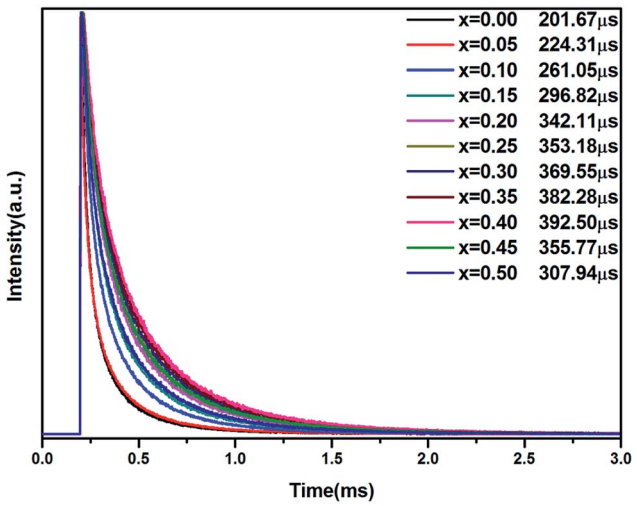

Fig. 7 Decay curves of LMZO:$Mn_{0.004}^{4+}$,Ga_x^{3+} ($x = 0.00$, 0.05, 0.10, 0.15, 0.20, 0.25, 0.30, 0.35, 0.40, 0.45, 0.50) phosphors ($\lambda_{ex} = 468$ nm; $\lambda_{em} = 670$ nm).

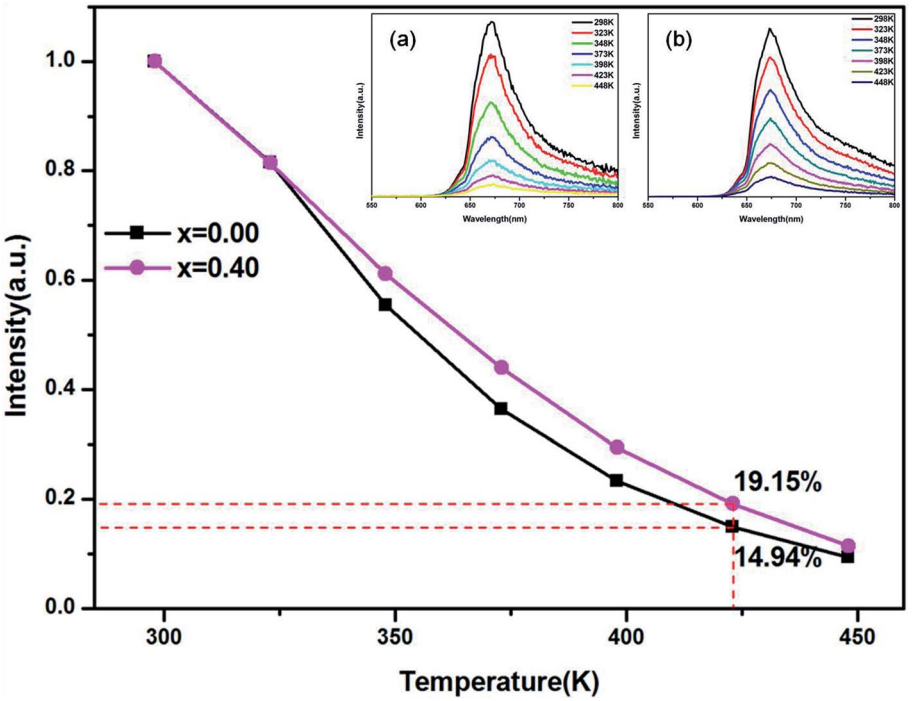

Fig. 8 Integrated emission intensity of the LMZO:$Mn_{0.04}^{4+}$,$Ga_{0.40}^{3+}$ and LMZO:$Mn_{0.004}^{4+}$,$Ga_{0.00}^{3+}$ phosphors under 468 nm excitation as a function of temperature. The inset: the temperature-dependent emission spectra of (a) LMZO:$Mn_{0.004}^{4+}$,$Ga_{0.00}^{3+}$ and (b) LMZO:$Mn_{0.004}^{4+}$,-$Ga_{0.40}^{3+}$ phosphors in the temperature range of 298–448 K.

where $I(t)$ is the time (t) dependent luminescence intensity at 670 nm. The calculated mean lifetimes for the samples of different Ga^{3+} concentration are given in Fig. 7. It is found that the decay time for the Mn^{4+} red emission exhibits an upward tendency with the increase of Ga^{3+} doping concentration. This could be ascribed to the reduced low valent Mn ions and thus the decreased luminescence quenching caused by the energy transfer between the Mn^{4+} ions and other low valent Mn ions. When the Ga^{3+} concentration exceeds 40%, however, impurities such as $LiGaO_2$ and MgO gradually form. Mn ions of different valences in these impurities and other defects produced in the impurity might increase the luminescence quenching of Mn^{4+} in the LMZO host and correspondingly shorten the luminescence lifetime of 670 nm.

QE is one of important performance indexes of phosphors. Therefore, QE of LMZO:$Mn_{0.04}^{4+}$,$Ga_{0.40}^{3+}$ phosphor under excitation of 468 nm has also been measured and the measured QE value is 25.3%. This indicates that the further research role is to improve its QE in order to get applications in W-LEDs.

Additionally, the thermal stability of the LMZO:$Mn_{0.04}^{4+}$,-$Ga_{0.40}^{3+}$ phosphor has also been studied. Fig. 8 shows the integrated emission intensity of the LMZO:$Mn_{0.04}^{4+}$,$Ga_{0.40}^{3+}$ and LMZO:$Mn_{0.004}^{4+}$,$Ga_{0.00}^{3+}$ phosphors under 468 nm excitation as a function of temperature. The temperature-dependent emission spectra of (a) LMZO:$Mn_{0.004}^{4+}$,$Ga_{0.00}^{3+}$ and (b) LMZO:$Mn_{0.004}^{4+}$,$Ga_{0.40}^{3+}$ phosphors in the temperature range of 298–448 K have also been given as insets in Fig. 8. As demonstrated in the insets of Fig. 8, the positions of the emission bands did not show any distinct change with increasing temperature, whereas the PL intensity gradually reduced owing to the thermal quenching effect. It can be seen that the PL intensity of LMZO:$Mn_{0.004}^{4+}$,$Ga_{0.40}^{3+}$ phosphor at 423 K was about 19.15% of that at room-temperature, which is better than the value of 14.94% of LMZO:$Mn_{0.04}^{4+}$,$Ga_{0.00}^{3+}$ phosphor. The result indicates that the thermal stability of the phosphor can also be improved after doping with Ga^{3+} ions.

The activation energy for the aforementioned thermal quenching can be determined by using the following equation:[52]

$$I_T = \frac{I_0}{1 + c \times \exp(-\Delta E/kT)} \quad (2)$$

where I_0 and I_T are the emission intensity at initial temperature and measured temperature T, respectively, c is constant, K is Boltzmann's constant and ΔE is the activation energy. After the linear fitting for the relationship between $\ln[(I_T/I_0) - 1]$ and $1/(kT)$, the activation energy can be obtained and it is 0.36 eV for LMZO:$Mn_{0.004}^{4+}$,$Ga_{0.40}^{3+}$ and 0.34 eV for LMZO:$Mn_{0.004}^{4+}$,-$Ga_{0.0}^{3+}$, respectively. This indicates that the activation energy has been slightly promoted by Ga^{3+} doping.

4. Conclusions

In summary, LMZO:$Mn_{0.004}^{4+}$,Ga_x^{3+} (x = 0.00, 0.05, 0.10, 0.15, 0.20, 0.25, 0.30, 0.35, 0.40, 0.45, 0.50) phosphors were synthesized *via* conventional high-temperature solid-state reaction and the influence of Ga^{3+} doping on luminescence properties of Mn^{4+} in LMZO has been investigated. The prepared phosphor can exhibit deep red emission in region of 620–800 nm with peak at 670 nm, under excitation of both ultraviolet-violet and

blue-green light from 300 to 550 nm. The luminescence intensity of LMZO:Mn^{4+} can be significantly improved by doping Ga^{3+} ions, especially under blue excitation. The optimum Ga^{3+} doping concentration of LMZO:$Mn_{0.004}{}^{4+}$,$Ga_x{}^{3+}$ is determined to be $x = 0.40$. At $x = 0.40$, the red emission of Mn^{4+} is enhanced by 6.68 times and 13.0 times under 352 nm and 468 nm excitation, respectively, as compared with the Ga^{3+} un-doped sample. Moreover, the thermal stability of the phosphor has also been improved with the introduction of Ga^{3+} ions. The improved luminescence performance is attributed to the enhanced stability of Mn^{4+} ions in the host and the lowered symmetry of Mn^{4+} sites because of Ga^{3+} doping. The work might provide important and meaningful reference to seek high-performance Mn^{4+} doped oxide phosphors for W-LEDs application based on blue-emitting InGaN chip.

Conflicts of interest

There are no conflicts to declare.

Acknowledgements

This work was supported by the National Science Foundation of China (No. 11674272 & 51372214) and the National Natural Science Foundation of China and Guangdong Province (U1401241).

Notes and references

1 P. Pust, V. Weiler, C. Hecht, A. Tucks, A. S. Wochnik, A. K. Henss, D. Wiechert, C. Scheu, P. J. Schmidt and W. Schnick, *Nat. Mater.*, 2014, **13**, 891–896.
2 K. Li, M. Shang, H. Lian and J. Lin, *J. Mater. Chem. C*, 2016, **4**, 5507–5530.
3 J. Y. Park, J. S. Joo, H. K. Yang and M. Kwak, *J. Alloys Compd.*, 2017, **714**, 390–396.
4 Y. Chen, F. Pan, M. Wang, X. Zhang, J. Wang, M. Wu and C. Wang, *J. Mater. Chem. C*, 2016, **4**, 2367–2373.
5 P. Pust, P. J. Schmidt and W. Schnick, *Nat. Mater.*, 2015, **14**, 454–458.
6 H. M. Zhu, C. C. Lin, W. Q. Luo, S. T. Shu, Z. G. Liu, Y. S. Liu, J. T. Kong, E. Ma, Y. G. Cao, R. S. Liu and X. Y. Chen, *Nat. Commun.*, 2014, **5**, 4312–4321.
7 J. S. Kim, P. E. Jeon, Y. H. Park, J. C. Choi, H. L. Park, G. C. Kim and T. W. Kim, *Appl. Phys. Lett.*, 2004, **85**, 3696–3698.
8 Z. D. Hao, Z. D. Zhang, Z. D. Zhang, Z. D. Sun, Z. D. Luo, Z. D. Lu and Z. D. Wang, *Appl. Phys. Lett.*, 2007, **90**, 261113.
9 Z. D. Xie, N. Hirosaki and N. Takeda, *Appl. Phys. Express*, 2009, **2**, 022401–022403.
10 J. Y. Han, W. B. Im, G. Y. Lee and D. Y. Jeon, *J. Mater. Chem. C*, 2012, **22**, 8739–8798.
11 W. Lv, W. Z. Lv, Q. Zhao, M. M. Jiao, B. Q. Shao and H. P. You, *Inorg. Chem.*, 2014, **53**, 11985–11990.
12 W. B. Park, S. P. Singh, C. Yoon and K. S. Sohn, *J. Mater. Chem.*, 2012, **22**, 14068–14075.
13 S. Yamada, H. Emoto, M. Ibukiyama and N. Hirosaki, *J. Eur. Ceram. Soc.*, 2012, **32**, 1355–1358.
14 Y. Q. Li, N. Hirosaki, R. J. Xie, T. Takeda and M. Mitomo, *Chem. Mater.*, 2008, **20**, 6704–6714.
15 X. Qin, X. W. Liu, W. Huang, M. Bettinelli and X. G. Liu, *Chem. Rev.*, 2017, **117**, 4488–4527.
16 J. S. Zhong, D. Q. Chen, Y. Zhou, Z. Y. Wan, M. Y. Ding, W. F. Bai and Z. G. Ji, *Dalton Trans.*, 2008, **45**, 4762–4770.
17 B. Wang, H. Lin, J. Xu, H. Chen and Y. S. Wang, *ACS Appl. Mater. Interfaces*, 2014, **6**, 22905–22913.
18 D. Q. Chen, Y. Zhou, W. Xu, J. S. Zhong, Z. G. Jia and W. D. Xiang, *J. Mater. Chem. C*, 2014, **4**, 1704–1712.
19 H. Chen, H. Lin, Q. M. Huang, F. Huang, J. Xu, B. Wang, Z. B. Lin, J. C. Zhou and Y. S. Wang, *J. Mater. Chem. C*, 2016, **4**, 2374–2381.
20 X. Ding, Q. Wang and Y. Wang, *Phys. Chem. Chem. Phys.*, 2016, **18**, 8088–8097.
21 X. Y. Jiang, Z. Chen, S. M. Huang, J. G. Wang and Y. X. Pan, *Dalton Trans.*, 2014, **43**, 9414–9418.
22 Y. K. Xu and S. Adachi, *J. Appl. Phys.*, 2014, **105**, 013525–013530.
23 T. Takahashi and S. Adachi, *J. Electrochem. Soc.*, 2008, **155**, E183–E188.
24 L. Huang, Y. W. Zhu, X. J. Zhang, R. Zou, F. J. Pan, J. Wang and M. M. Wu, *Chem. Mater.*, 2016, **28**, 1495–1502.
25 J. S. Zhong, D. Q. Chen, X. Wang, L. F. Chen, H. Yu, Z. G. Ji and W. D. Xiang, *J. Alloys Compd.*, 2016, **662**, 232–239.
26 B. Wang, H. Lin, F. Huang, J. Xu, H. Chen, Z. B. Lin and Y. S. Wang, *Chem. Mater.*, 2016, **28**, 3515–3524.
27 R. P. Cao, J. J. Huang, X. F. Ceng, Z. Y. Luo, W. Ruan and Q. L. Hu, *Ceram. Int.*, 2016, **42**, 13296–13300.
28 Y. H. Jin, Y. H. Hu, H. Y. Wu, H. Duan, L. Chen, Y. R. Fu, G. F. Ju, Z. F. Mu and M. He, *Chem. Eng. J.*, 2016, **288**, 596–607.
29 D. Q. Chen, S. Liu, Y. Zhou, Z. Y. Wan, P. Huang and Z. G. Jia, *J. Mater. Chem. C*, 2016, **4**, 9044–9048.
30 W. Shu, L. L. Jiang, S. G. Xiao, X. L. Yang and J. W. Ding, *Mater. Sci. Eng., B*, 2012, **177**, 274–277.
31 K. Seki, S. Kamei, K. Uematsu, T. Ishigaki, K. Toda and M. Sato, *J. Ceram. Process Res.*, 2013, **14**, s67–s70.
32 Z. X. Qiu, T. T. Luo, J. L. Zhang, W. L. Zhou, L. P. Yu and S. X. Xun, *J. Lumin.*, 2015, **158**, 130–135.
33 S. J. Lee, J. Jung, J. Y. Park, H. M. Jang, Y. R. Kim and J. K. Park, *Mater. Lett.*, 2013, **111**, 108–111.
34 E. Ö ztürk and N. O. Kalaycioglu, *Mater. Res. Bull.*, 2012, **47**, 1138–1141.
35 E. Ö ztürk and N. O. Kalaycioglu, *Solid State Phenom.*, 2015, **230**, 217–220.
36 E. Circir and N. O. Kalaycioglu, *J. Therm. Anal. Calorim.*, 2012, **110**, 1179–1183.
37 N. O. Kalaycioglu and E. Ö ztürk, *J. Therm. Anal. Calorim.*, 2012, **111**, 273–277.
38 E. Ö ztürk, N. O. Kalaycioglu and S. Dayan, *J. Therm. Anal. Calorim.*, 2014, **117**, 573–578.
39 R. Cao, Z. Shi, G. Quan, T. Chen, S. Guo, Z. Hu and P. Liu, *J. Lumin.*, 2017, **188**, 577–581.

40 M. Castellanos, A. R. West and W. B. Reid, *Acta Crystallogr., Sect. C: Cryst. Struct. Commun.*, 2016, **41**, 1707–1709.
41 R. D. Shannon, *Acta Crystallogr., Sect. A: Cryst. Phys., Diffr., Theor. Gen. Crystallogr.*, 2016, **32**, 751–767.
42 T. Sasaki, J. Fukushima, Y. Hayashi and H. Takizawa, *J. Lumin.*, 2017, **188**, 101–106.
43 L. Chen, X. Deng, E. Zhao, X. Chen, S. Xue, W. Zhang, S. Chen, Z. Zhao, W. Zhang and T.-S. Chan, *J. Alloys Compd.*, 2014, **613**, 312–316.
44 Y. Chen, M. Wang, J. Wang, M. M. Wu and C. X. Wang, *J. Solid State Light.*, 2014, **1**, 15.
45 M. Brik, S. Camardello and A. Srivastava, *ECS J. Solid State Sci. Technol.*, 2015, **4**, R39–R43.
46 K. Li, H. Lian and R. V. Deun, *Dalton Trans.*, 2017, **00**, 1–4.
47 L. Li, Y. Pan, Z. Chen, S. Huang and M. Wu, *RSC Adv.*, 2017, **7**, 14868–14875.
48 M. Medic, M. Brik, G. Dražić, Ž. Antić, V. Lojpur and M. Dramićanin, *J. Phys. Chem. C*, 2015, **119**, 724–730.
49 R. Cao, J. Zhang, W. Wang, Z. Hu, T. Chen, Y. Ye and X. Yu, *Mater. Res. Bull.*, 2017, **87**, 109–113.
50 L. Wang, Z. Dai, R. Zhou, B. Qu and X. C. Zeng, *Phys. Chem. Chem. Phys.*, 2018, **20**, 16992–16999.
51 H. Jing, C. Guo, G. Zhang, X. Su, Z. Yang and J. H. Jeong, *J. Mater. Chem.*, 2012, **22**, 13612–13618.
52 S. Bhushan and M. Chukichev, *J. Mater. Sci. Lett.*, 1988, **7**, 319–321.